JOURNAL OF THE ROYAL SOCIETY Interface

Adhesion and sliding response of a biologically inspired fibrillar surface: experimental observations

H Yao, G. Della Rocca, P.R Guduru and H Gao

J. R. Soc. Interface 2008 **5**, 723-733
doi: 10.1098/rsif.2007.1225

JOURNAL OF THE ROYAL SOCIETY Interface

J. R. Soc. Interface (2008) **5**, 723–733
doi:10.1098/rsif.2007.1225
Published online 30 October 2007

Adhesion and sliding response of a biologically inspired fibrillar surface: experimental observations

H. Yao, G. Della Rocca, P. R. Guduru* and H. Gao

Division of Engineering, Brown University, Providence, RI 02912, USA

Inspired by the adhesion mechanisms of several animal species such as geckos, beetles and flies, several efforts in designing and fabricating surface engineering strategies have been made recently to mimic the adhesive and frictional behaviour of biological foot pads. An important feature of such biological adhesion systems is the ability to switch between strong attachment and easy detachment, which is crucial for animal locomotion. Recent investigations have suggested that such a 'switching' mechanism can be achieved by the elastic anisotropy of the attachment pad, which renders the magnitude of the detachment force to be direction dependent. This suggestion is supported by the observations that the fibres of the foot pads in geckos and insects are oriented at an angle to the base and that geckos curl their toes backwards (digital hyperextension) while detaching from a surface. One of the promising bio-inspired architectures developed recently is a film-terminated fibrillar PDMS surface; this structure was demonstrated to result in superior detachment force and energy dissipation compared with a bulk PDMS surface. In this investigation, the film-terminated fibrillar architecture is modified by tilting the fibres to make the surface vertically more compliant and elastically anisotropic. The directional detachment and the sliding resistance between the tilted fibrillar surfaces and a spherical glass lens are measured: both show significant directional anisotropy. It is argued that the anisotropy introduced by the tilted fibres and the deformation-induced change in the compliance of the fibre layer are responsible for the observed anisotropy in the detachment force.

Keywords: gecko adhesion; fibrillar surface; anisotropic adhesion; anisotropic friction

1. INTRODUCTION

Recent work (Autumn *et al.* 2000) has demonstrated that the micro- and nanoscale architectures of gecko foot fibres are responsible for the animal's excellent attachment capability; this work has led to several investigations describing the mechanics of insect attachment as well as creating surface engineering strategies to mimic it (Jagota & Bennison 2002; Arzt *et al.* 2003; Gao *et al.* 2003, 2005; Geim *et al.* 2003; Persson & Gorb 2003; Hui *et al.* 2004; Peressadko & Gorb 2004; Crosby *et al.* 2005; Huber *et al.* 2005; Northen & Turner 2005, 2006; Persson *et al.* 2005; Spolenak *et al.* 2005*a*,*b*; Tang *et al.* 2005; Yurdumakan *et al.* 2005; Bhushan *et al.* 2006; Kim & Sitti 2006; Tian *et al.* 2006; Yao & Gao 2006; Zhao *et al.* 2006; Glassmaker *et al.* 2007; Gorb *et al.* 2007; Kim & Bhushan 2007). For example, Kim & Sitti (2006) fabricated arrays of polyurethane elastomer microfibres with spatulate tips and demonstrated that their pull-off force is over four times that of a flat surface of the same material. In a recent paper, Gorb *et al.* (2007) showed that a surface of polyvinylsiloxane fibres with mushroom-shaped tips results in an increase in the pull-off force by more than a factor of 2. Bhushan & Sayer (2007) measured the coefficient of kinetic friction of a similar mushroom fibre surface to be about four times that of a reference unstructured surface. Crosby *et al.* (2005) showed that adhesion can be increased by up to 400% by fabricating patterns of low aspect ratio post structures on a surface. Yurdumakan *et al.* (2005) explored the possibility of using aligned carbon nanotube surfaces by measuring the adhesion of the end of a nanotube to the tip of an atomic force microscope cantilever. Zhao *et al.* (2006) developed vertically aligned carbon nanotube surfaces whose adhesion and shear strength were comparable to those of a gecko foot. More recently, Ge *et al.* (2007) showed that patterned carbon nanotube surfaces could support shear loads four times as much as a natural gecko foot. Glassmaker *et al.* (2007) developed a bio-inspired architecture where a vertical array of PDMS microfibres terminates in a continuous PDMS thin film and showed that the pull-off force and the work of adhesion can be increased several times over those of a bulk PDMS surface by properly choosing the geometrical parameters, such as the fibre aspect ratio, spacing, film thickness, etc. They also carried out a detailed analysis

*Author for correspondence (pradeep_guduru@brown.edu).

Received 11 September 2007
Accepted 4 October 2007

of adhesion between the film-terminated vertical fibrillar surface and a glass sphere and explained the increase in adhesion in terms of a crack-trapping mechanism due to fluctuating energy release rate along the interfacial crack path.

A key feature of gecko and other insect attachment is the ability to quickly switch between strong adhesion and easy detachment, essential in locomotion. It is generally recognized that the fibre geometry and the fibre tip geometry play an important role in such a switching mechanism. In an analysis of gecko adhesion mechanisms, Persson *et al.* (2005) argued that the tilted orientation of the gecko setae plays an important role in enhancing adhesion by increasing the normal compliance of the fibrillar foot pad. Such an argument suggests that tilting the fibres with respect to the surface normal in the architecture of Glassmaker *et al.* (2007) should result in an improved adhesion performance. Gao *et al.* (2005) showed that the asymmetric shape of spatula tip makes the magnitude of the adhesion force to be a function of its direction of application. Based on their analysis, they suggested that the tip shape of the fibres offers a possible switching mechanism between robust adhesion and easy detachment. Also, Sitti & Fearing (2003) proposed a model which predicts that the friction of a slanted fibre tip will be a function of sliding direction, and speculated that such anisotropy could provide a possible release mechanism. The effect of fibre orientation on making adhesion and friction anisotropic was recognized by Autumn *et al.* (2000) as well during their measurements on actual gecko setae.

Further, assuming that arrays of tilted fibres can be viewed as an anisotropic elastic continuum, Yao & Gao (2006) studied the conditions for the growth of a crack at the interface between rigid and elastic transversely isotropic half-spaces and showed that the critical far-field traction for crack propagation is direction dependent. It was shown to be maximum along the 'stiff' direction (direction of maximum elastic modulus) and minimum along the 'compliant' direction (direction of minimum elastic modulus). The ratio of the maximum to the minimum was shown to be proportional to the 1/4th power of the ratio of the elastic moduli in the respective directions. Later, Chen & Gao (2007) studied the adhesion of a cylinder to an elastic transversely isotropic half-space and showed that the pull-off force shows a sharp maximum along the stiff direction and a shallow minimum along the compliant direction. These analyses suggest that the fibre orientation in an insect foot pad provides another possible switching mechanism between the adhered and detached states. Thus, a film-terminated tilted fibre architecture is expected to possess not only an improved detachment force but also anisotropic adhesion and sliding response, which are of practical interest in designing and fabricating biomimetic surfaces for optimized adhesion and friction performance.

This article describes an experimental investigation of direction-dependent adhesion and sliding response of a film-terminated fibre array architecture in which the fibres are tilted with respect to the surface normal. The main observations of this investigation are as follows: (i) the pull-off force increases with fibre tilt angle, (ii) there exists a direction of minimum pull-off force, which tends to become sharp with increase in fibre tilt angle, and (iii) under constant tensile normal force, fibrillar surfaces show highly anisotropic sliding resistance.

2. SAMPLE DESCRIPTION AND PREPARATION

The structure of the sample is schematically illustrated in figure 1*a*. It is similar in architecture to that of Glassmaker *et al.* (2007) except that the fibres are tilted with respect to the surface normal by an angle ϕ. Also, the dimensions (fibre diameter, height, spacing, film thickness, etc.) are much larger than those employed by Glassmaker *et al.* (2007). Since the primary objective of this investigation is to establish the behaviour of the tilted fibre system, the dimensions are chosen based on ease and convenience of fabrication. The observed response is expected to carry over to smaller scales as well.

The first step in sample fabrication is to prepare a Teflon mould with a two-dimensional array of oblique holes by conventional drilling. The thickness of the Teflon sheet is 1.5 mm; each hole is 250 μm in diameter and the normal distance between central axes of two adjacent holes is 500 μm. A typical dimension of the hole array is 21×21. A 10 : 1 ratio of Sylgard 184 silicone elastomer base and curing agent was mixed, degassed and poured on the Teflon mould in low vacuum. The samples were then cured in an oven at 75°C for 2 hours. Careful demoulding was necessary to avoid fibre breakage. In order to fabricate the film on top of the fibres, PDMS was poured on a clean silicon wafer and was spun at a speed of $500g$ for 60 s, with an initial acceleration of $50g\ \mathrm{s}^{-1}$. The average thickness of the film obtained is 125 μm. The tips of the fibre array were then placed on top of the PDMS film, while making sure that all the fibre tips were in contact with the PDMS film. The assembly was then cured for 16 hours at 75°C during which the fibre tips bond with the PDMS film. The fibre array, along with the terminal film, was then peeled off from the silicon wafer. A photograph of the sample obtained is shown in figure 1*d*.

3. EXPERIMENTAL SET-UP

The measurement of the adhesion and lateral forces was made with a microtribometer, designed and built in-house, as shown in figure 1*b*. The measurement procedure is similar to that employed by Liu & Bhushan (2003) and Rennie *et al.* (2005). A stainless steel cantilever with two arms acts as a two-dimensional force transducer, as shown in figure 1*c*. The normal and lateral spring constants of the cantilever are 2334 and $5238\ \mathrm{N\ m}^{-1}$, respectively. Normal and lateral forces were measured indirectly by measuring the deflection of the cantilever tip with fibre optic displacement sensors (Philtec, Model: D20). A pair of perpendicular mirrors is located on the cantilever tip as shown in figure 1*c*, which provides reflecting surfaces for the displacement sensors. Within the range of operation, the output sensitivity of the sensors is approximately $10\ \mathrm{mV\ \mu m}^{-1}$. The crosstalk between the normal and lateral force measurements has been measured to be less than 1%. The output signals are

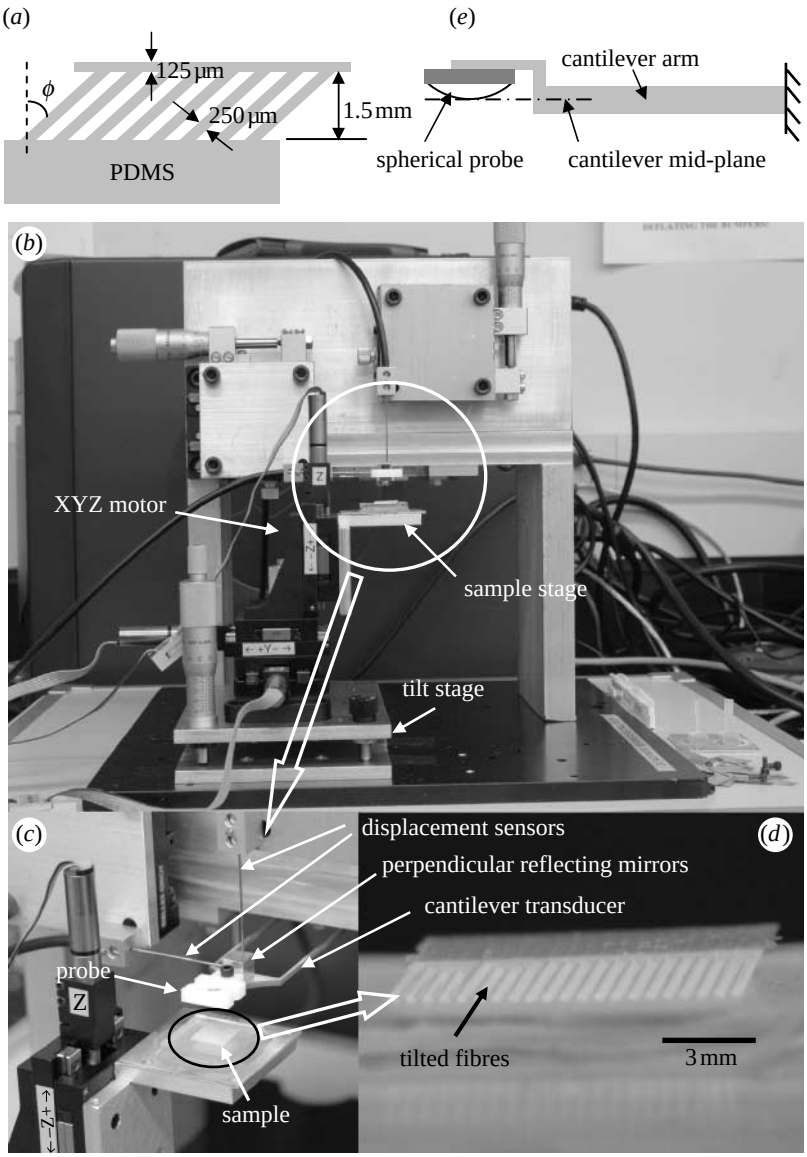

Figure 1. (*a*) Schematic illustration of the geometry of the film-terminated tilted fibre samples. (*b*) A photograph of the set-up to measure normal and lateral forces during directional adhesion and sliding experiments. (*c*) A detailed view of the sample, probe, cantilever and displacement sensors. (*d*) A photograph of the film-terminated tilted fibre sample. (*e*) Schematic illustration of the cantilever and spherical probe assembly in which the bottom plane of the probe coincides with the mid-plane of the cantilever in order to minimize crosstalk between the normal and the lateral force measurements.

digitized with a 14 bit analogue to digital converter and sampled at 20 Hz. The signal noise is 0.3 mV. Hence, cantilever displacements as small as 30 nm can be detected. The smallest detectable change in force can be tuned by changing the cantilever dimensions to modify the cantilever spring constant. In the current experiments, the stiffness was chosen such that the maximum cantilever deflection was not greater than 200 µm.

The probe is a glass lens of radius 103.4 mm, which is attached to the cantilever end as shown in figure 1. The radius was chosen such that the area of contact is sufficiently large to contain several fibre tips, and the observed adhesive and frictional behaviour represents an averaged response of the fibrous layer. The glass lens is attached in such a way that its bottom plane lies in the mid-plane of the cantilever, as illustrated in figure 1*e*. This design minimizes crosstalk between the lateral and normal force measurements. The digitized signals are acquired with LabView (National Instruments, Austin, TX) software. Samples are mounted on a motorized XYZ stage (Thorlabs, Inc., model: T25 XYZ-E/M), which has a displacement resolution of 50 nm. However, when the direction of travel is reversed, the backlash is 1–2 µm. The stage can be programmed to follow any three-dimensional trajectory through simultaneous control of all three axes. LabView routines are used to control the motors and to synchronize data acquisition with sample motion. The entire device is placed on a vibration isolation platform. In order to assess the anisotropic adhesion and friction behaviour of the tilted fibre samples, two types of experiments were carried out, as described below.

3.1. Directional adhesion experiments

In these experiments, the sample is separated from the probe at a constant speed $v=3\ \mu m\ s^{-1}$ until pull-off at angles spanning $-90^\circ<\theta<90^\circ$ in the y–z plane as

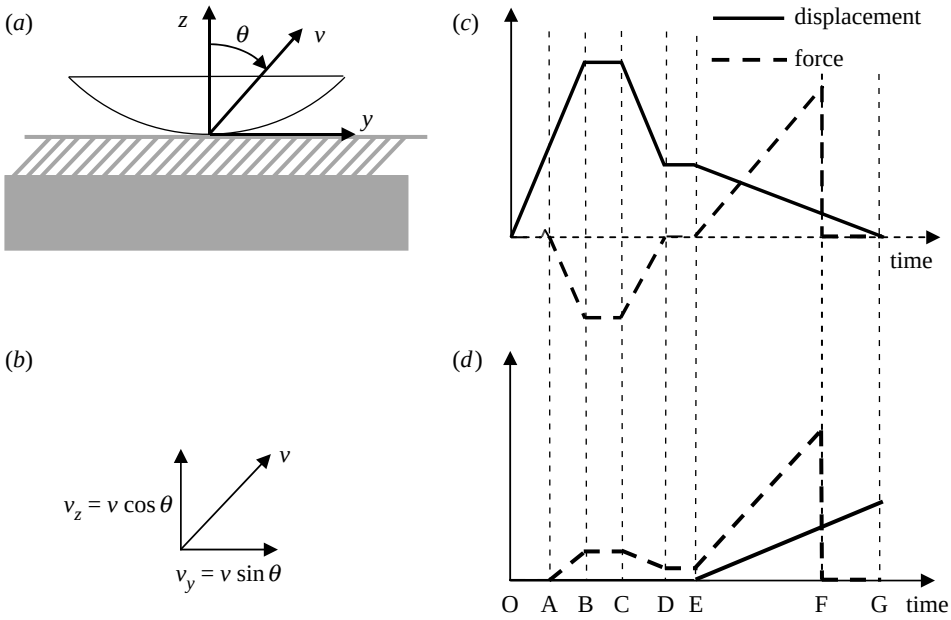

Figure 2. Schematic illustration of the directional adhesion experiment. The plots illustrate the displacement and force histories during a typical experiment. (*a*) The spherical probe is separated from the sample surface at an angle θ from the normal, at a velocity v. (*b*) It is accomplished by moving the stage in y- and z-directions simultaneously at the component velocities v_z and v_y. (*c*) Displacement and force in the normal direction (z). (*d*) Displacement and force in the lateral (y) direction. The sample approaches the probe normally and contacts it around A. Normal approach continues until a fixed preload is reached at B. At C, the sample retracts from the probe normally until D, when the normal force becomes zero. At E, the sample stage starts moving simultaneously in y- and z-directions. At F, the probe pulls off and the forces drop to zero.

illustrated in figure 2*a*. The angle θ is taken to be positive in the orientation shown in figure 2*a*. Figure 2*c* illustrates details of initial attachment and the subsequent separation process: these schematic plots are time histories of displacement and force in the normal and lateral directions, respectively. A typical experiment is initiated at time O when the probe and the sample are not in contact. The sample approaches the probe normally ($\theta = 0°$) and contacts it around A, which is associated with a 'pull-in' instability. The corresponding pull-in kink in the force is illustrated in figure 2*c*. Normal approach continues until a fixed compressive preload is reached, at point B. At point C, the sample retracts from the probe normally until D, when the normal force becomes zero. At E, the sample stage starts moving simultaneously in the y- and z-directions at velocities v_y and v_z, respectively, as shown in figure 2*b*. This movement results in a separation velocity v at an angle θ. At F, the probe pulls off and both force components drop sharply to zero. Alternatively, when θ is close to 90°, the pull-off and the sharp drops in the forces shown in figure 2 are replaced by stick–slip and the corresponding force oscillations, respectively. Note that during AB and CD, even though there is only normal displacement, the lateral force changes owing to the elastic anisotropy of the tilted fibre layer.

3.2. Sliding under tensile force

In these experiments, the sample is moved laterally at a constant velocity $v = 3\ \mu m\ s^{-1}$ with a constant tensile force P between the sample and the probe. The history of displacement and force in a typical experiment is shown in figure 3. The lateral or tangential force is taken to be positive if the sphere is sliding in the positive y-direction with respect to the sample, i.e. in the direction of fibre tilt, and is negative in the opposite direction. The sequence of events from O to D is the same as in the directional adhesion experiment, except that the force at D is now tensile and has a magnitude P. Owing to elastic anisotropy of tilted fibre layer, lateral force is non-zero at D. At E, the sample starts moving laterally at a velocity v. During this lateral motion, the z-position of the sample is continuously adjusted to hold the normal force constant. Hence, the normal displacement is shown as a dotted line in figure 3*b*. To maintain a constant tensile force, the z-position is adjusted through a feedback control algorithm, implemented in LabView. At F, the probe pulls off, resulting in a sharp drop-off in both the force components to zero. Alternatively, if stick–slip occurs, such drop in lateral force is replaced by the corresponding force oscillations.

4. EXPERIMENTAL RESULTS

4.1. Directional adhesion experiments

To study adhesion and friction response of the tilted fibre samples, four values were chosen for the fibre tilt angle ϕ shown in figure 1*a*: $\phi = 0°$, 20°, 30° and 40°. In addition, bulk PDMS samples were also prepared for reference. To ensure that the bulk sample surface is identical to the top surface of the fibrillar samples, a thin PDMS film was transferred to the top of the bulk sample using the same procedure as that for the fibrillar samples. The detachment force, along with its normal and tangential components, of directional adhesion experiment on bulk PDMS is shown in figure 4*a*. Note the expected symmetry of the

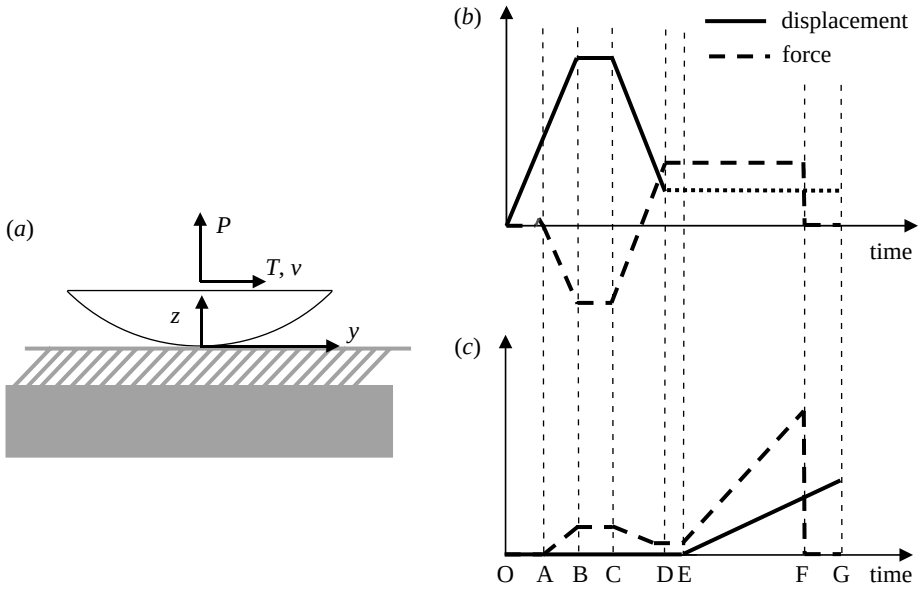

Figure 3. Schematic illustration of the 'sliding under tensile force' experiment. The plots illustrate the displacement and force histories during a typical experiment. (*a*) The spherical probe is moved laterally at a velocity v while holding the normal tensile force P constant. The corresponding lateral force is T. (*b*) Displacement and force histories in the normal direction (z). (*c*) Displacement and force histories in the lateral (y) direction. The sequence of events from O to D are the same as given in figure 2, except the force at D is now tensile and has a magnitude P. Owing to elastic anisotropy of tilted fibre layer, lateral force is non-zero at D. At E, the sample stage starts moving laterally at a velocity v while the normal force P is held constant. The probe pulls off at F.

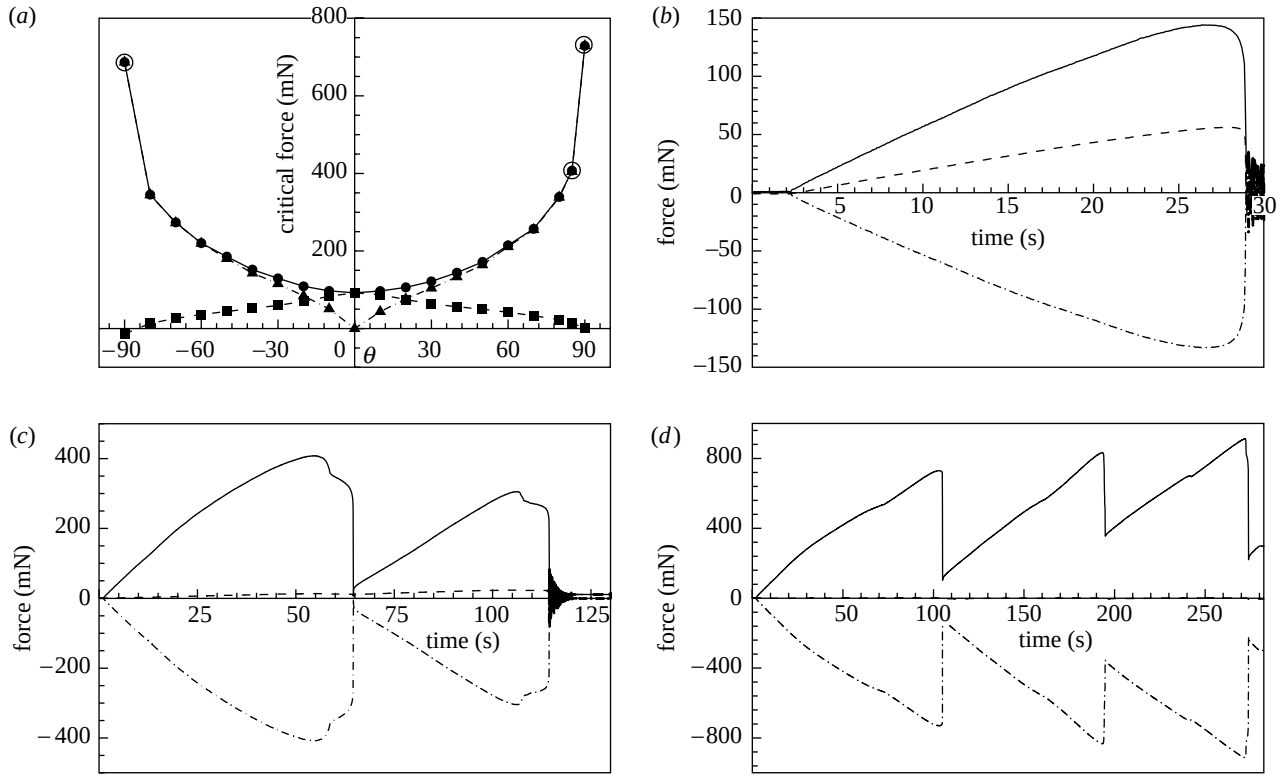

Figure 4. (*a*) Directional adhesion response of bulk PDMS, showing the variation of total detachment force and its normal and lateral components as a function of the separation angle θ. Note that the total force is the magnitude of the force vector at pull-off/sliding. The measurement uncertainty is approximately 5%. The error bars are omitted for clarity (soild square, dashed line, normal; solid triangle, dashed, dot line, lateral; solid circle, solid line, total; open circle, stick–slip). (*b*) Force versus time plot for $\theta = 40°$, showing monotonic increase in forces until pull-off (dashed line, normal; dashed, dot line, lateral; solid line, total). (*c*) Stick–slip instabilities for $\theta = 85°$, before pull-off (dashed line, normal; dashed, dot line, lateral; solid line, total). (*d*) For $\theta = 90°$, the normal force remains close to zero and the stick–slip instabilities persist without a clean pull-off separation (dashed line, normal; dashed, dot line, lateral; solid line, total).

data about $\theta = 0°$, where the detachment force is minimum. As θ increases, the normal component decreases while the tangential component increases. The normal component decreases to zero as θ gets close to 90°. A plot of force versus time for $\theta = 40°$ is shown in figure 4*b*, which is qualitatively representative of all

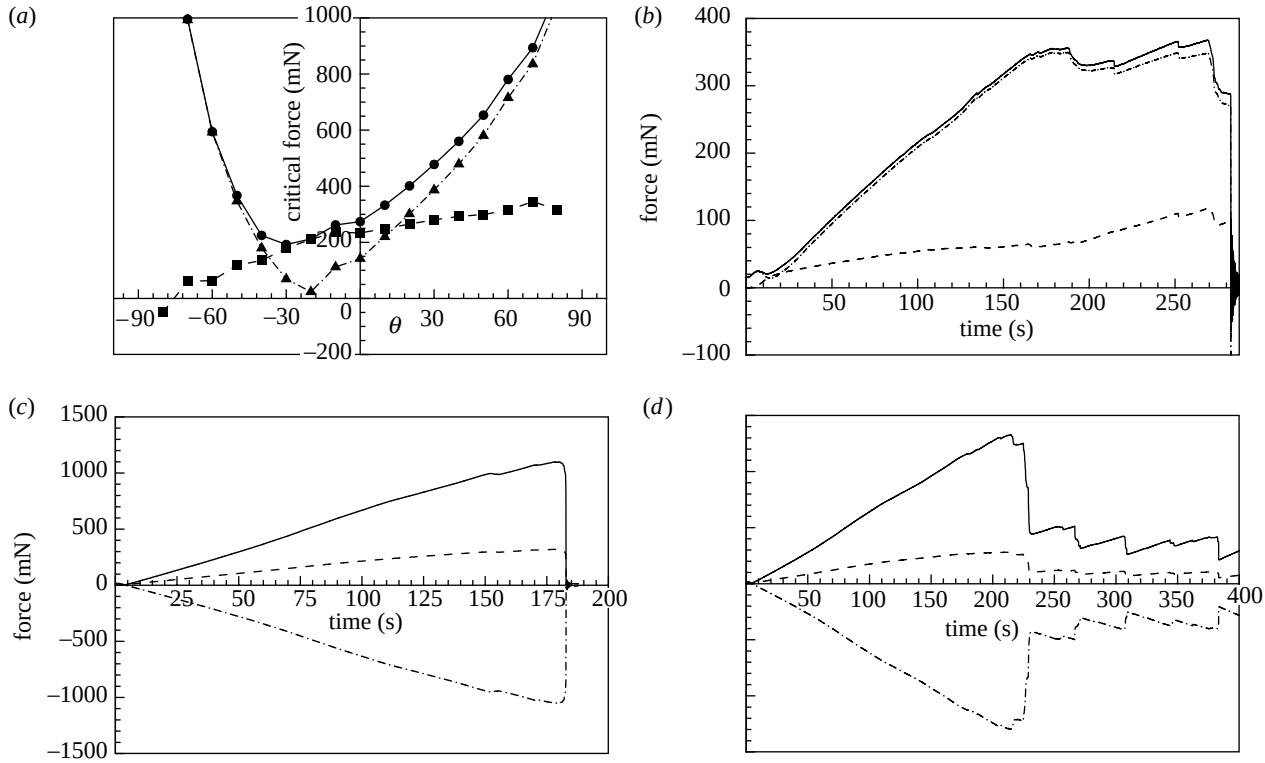

Figure 5. (*a*) Directional adhesion response of 40° tilted fibre sample, showing the variation of detachment force and its normal and tangential components as a function of the separation angle θ. The total force is the magnitude of the force vector at pull-off/sliding. Note that the total detachment force is minimum at an angle of approximately $-30°$. Also, the normal component continuously increases with θ. The measurement uncertainly is $\pm 5\%$. Error bars are omitted for clarity (soild square, dashed line, normal; solid triangle, dashed, dot line, lateral; solid circle, solid line, total). (*b*) Force versus time plot for $\theta = -50°$, showing discrete slip events before final pull-off (dashed line, normal; dashed, dot line, lateral; solid line, total). (*c*) Force versus time for $\theta = 80°$, showing an almost monotonic increase in forces until pull-off even at such a high angle. (dashed line, normal; dashed, dot line, lateral; solid line, total). (*d*) Stick–slip behaviour for $\theta = 90°$ (dashed line, normal; dashed, dot line, lateral; solid line, total).

angles $|\theta| \leq 80°$. Both normal and tangential force components increase monotonically and reach a maximum before unstable separation or pull-off. The detail of interfacial processes such as propagation of slip, etc., in such a single asperity contact subjected to simultaneous normal and tangential forces has been a subject of several past investigations (Savkoor 1987; Israelachvili 1992; Carpick *et al.* 1996; Johnson 1997; Kim *et al.* 1998). A discussion of these issues is deliberately omitted here since the immediate objective of this article is to examine the performance of the fibrillar surface architecture; the bulk sample is tested merely to provide a reference for the performance of the fibrillar surfaces. When $|\theta| > 80°$, the separation process transitions to stick–slip regime as shown in figure 4*c*,*d* for $\theta = 85°$ and 90°, respectively. In figure 4*c*, since the surfaces are normally moving away from each other due to the normal component of the separation velocity, the normal tensile force builds up slowly and the two surfaces pull off with respect to each other after a few stick–slip cycles. However in figure 4*d*, since the relative displacement is nominally parallel to the surfaces, the increase in the normal force is negligible and the stick–slip process appears to continue indefinitely.

It is interesting to note that the magnitude of the detachment force increases substantially as a function of θ, as seen in figure 4*a*. Assuming that pull-off at an oblique angle is governed by a critical energy release rate criterion (similar to the JKR model), the most likely explanation for the increase in the detachment force for bulk PDMS as a function of the angle of detachment θ is the dependence of the critical energy release rate (or interface toughness) at the contact periphery on mode mixity. As θ increases, sliding (mode II and III) component at the contact periphery increases. In fracture mechanics of adhesive joints, it is well known that the interface toughness increases rapidly as a function of the mode-mixity parameter $\tan^{-1}(K_{\mathrm{II}}/K_{\mathrm{I}})$, where K_{II} and K_{I} are the mode II and mode I stress intensity factors, respectively. For example, Liechti & Chai (1992) showed that the interface toughness of a glass–epoxy interface can increase by an order of magnitude when a significant sliding component is present. Some of the possible mechanisms for such an increase include inelastic dissipation, microbranching, asperity interlocking and frictional dissipation. A similar increase in the interface toughness for the adhesive contact in our experiments between the glass sphere and PDMS can explain the observed increase in detachment force in figure 4*a*. However, the dependence of interface toughness on mode mixity for such an adhesive contact has not been measured before and remains an open problem. A detailed investigation on this issue is currently underway by the authors, which will be reported separately.

Figure 5 is a similar summary of the directional adhesion results for the 40° tilted fibre samples. The main features of the response are as follows. (i) The detachment force has a relatively sharp valley near

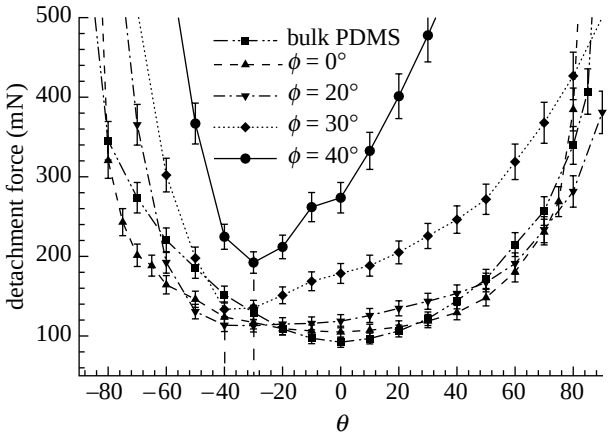

Figure 6. Summary of directional adhesion experiments. The detachment force increases with fibre tilt angle ϕ. Also, the shape of the curve near the minimum becomes sharp as the tilt angle increases. The sharp minimum suggests that it can serve as an easy detachment direction.

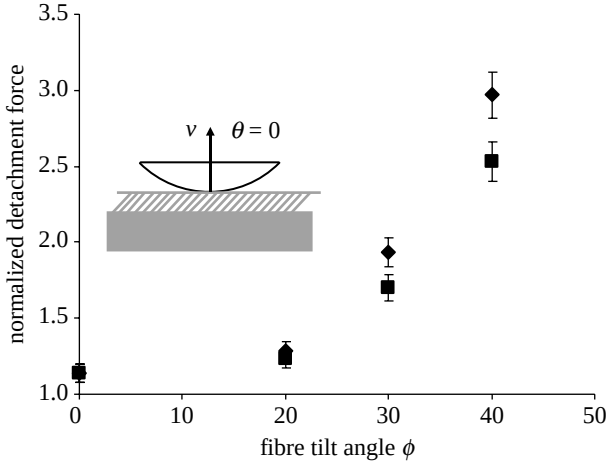

Figure 7. Normalized detachment force along $\theta = 0°$, as a function of the fibre tilt angle ϕ. The detachment force is normalized with the normal pull-off force for bulk PDMS. The plot shows the total detachment force as well as its normal component (solid diamond, total force; solid square, normal component).

$\theta = -30°$ (the values of θ are taken to be positive towards fibre tilt, as shown in figure 2*a*), which can serve as a direction of easy detachment. (ii) The magnitude of the normal component increases almost monotonically with θ. Unlike the bulk samples, the tilted fibre sample can retain its normal attachment capability even under relatively large tangential forces. (iii) For positive angles as high as 80°, the interface undergoes pull-off separation without stick–slip as shown in figure 5*c*. Stick–slip response for $\theta = +90°$ is shown in figure 5*d*; the interface does not regain its stick-strength after the initial slip. A typical force curve for negative angles is shown in figure 5*b* for $\theta = -50°$, which is characterized by several small slip events before pull-off. A summary of directional adhesion experiments for all cases considered is shown in figure 6. Here, the features described above for the 40° sample seem to generally hold for other angles as well, with a gradual transition between $\phi = 0°$ and 40°. Note that, as

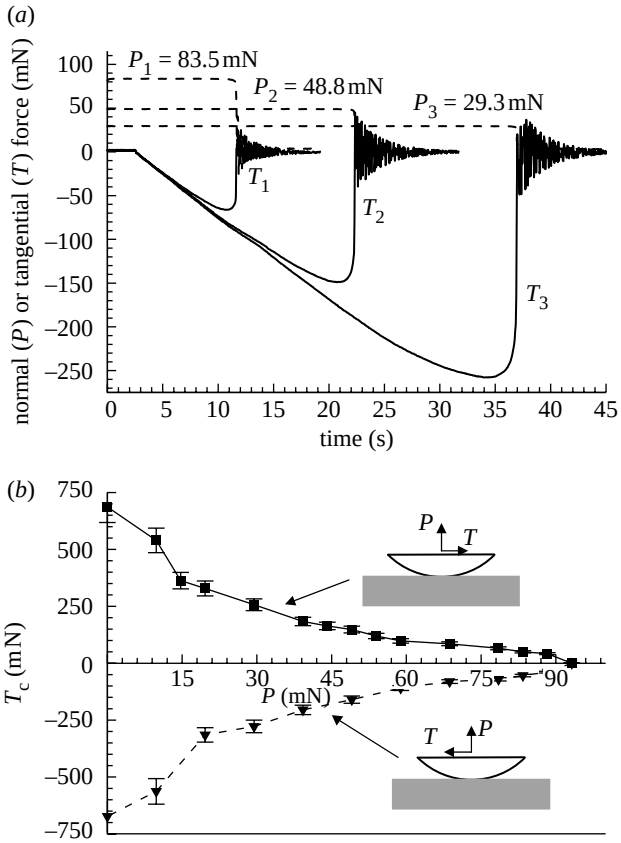

Figure 8. Sliding under tensile force—results for bulk PDMS. (*a*) History of normal force P and tangential force T for three different values of P. The dashed and solid lines represent P and T, respectively. As P decreases, critical T at pull-off, T_c, increases. (*b*) Critical tangential force T_c as a function of the tensile normal force P. The inset figures show the direction of sliding. Note that the increase in T_c is gradual and almost linear over most of the range of P except at the extreme left.

the fibre tilt angle ϕ increases, the detachment force increases significantly over a substantial range of θ. This observation is shown in figure 7, which plots the normalized detachment force and its normal component with $\theta = 0°$ for the four values of ϕ considered. The forces are normalized with the normal ($\theta = 0°$) pull-off force for the bulk sample. For $\phi = 0°$, the improvement in adhesion is only marginal. This result is consistent with the work of Glassmaker *et al.* (2007) who showed that significant enhancement in adhesion with vertical fibres is realized only for certain range of parameters, such as fibre aspect ratio, film thickness, fibre spacing, etc. Thus, it is not surprising that the adhesion of the vertical fibre sample used here results in only marginal increase in pull-off force. Increases in detachment force appear to become substantial beyond $\phi = 20°$; for the 40° sample, the total detachment force is three times and its normal component is approximately 2.5 times that of the bulk sample. These results demonstrate that the tilted fibre architecture is an effective biologically inspired surface engineering strategy to realize strong adhesion. By optimizing the geometric parameters, it should be possible to realize even greater enhancement than the results shown here.

A comment on the fibre tilt angle is necessary in the context of the above experiments. θ is the direction of

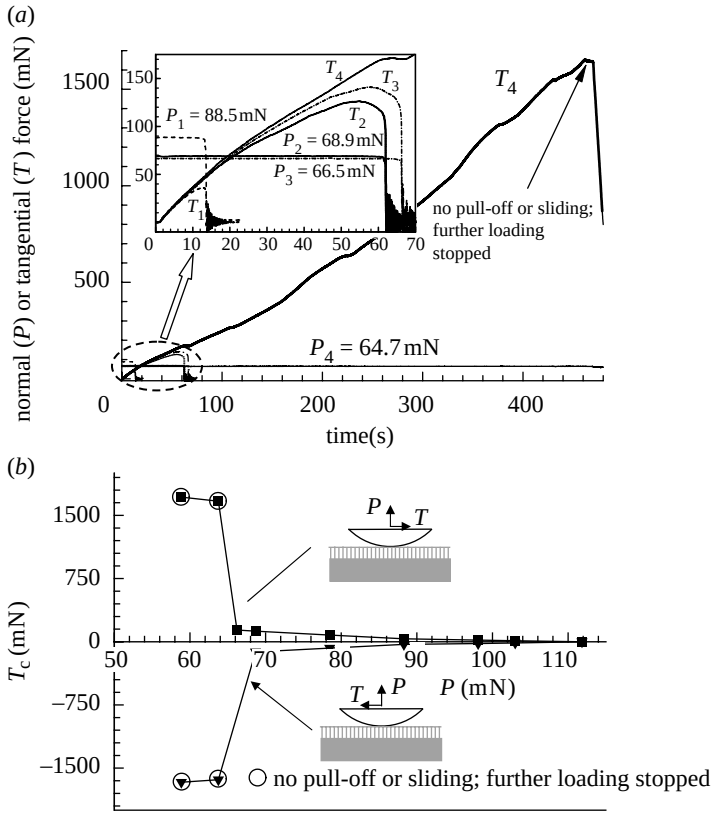

Figure 9. Sliding under tensile force—results for vertical fibre samples ($\phi=0°$). (*a*) History of normal (P) and tangential (T) forces during sliding. The inset shows a detailed view of the plots at the lower left corner. For $P=66.5$ mN and above, T increases as in the bulk PDMS case and the surfaces pull off at critical T_c. However, for a slightly lower $P=64.7$ mN, the contact area expands with lateral motion and the interface can sustain an order of magnitude higher T without slip. At the highest value of T (approx. 1650 mN), there was neither separation nor relative sliding. Further loading was stopped to prevent fibre fracture. (*b*) Critical tangential force T_c as a function of normal tensile force. Note the steep increase in T_c in contrast to the bulk PDMS case. The estimated measurement error is $\pm 5\%$.

the spherical probe and ϕ is the 'initial' fibre tilt angle. When the spherical probe is retracted, the fibre tilt angle does change within the area of contact; it remains unchanged away from the area of contact and gradually varies in between. Clearly, θ can be controlled independently. However, the fibre tilt angle changes during attachment and detachment, by different amounts in different parts of the sample. While presenting the results for samples with particular value of ϕ, it is not implied that the fibre tilt angle remains fixed and independent of θ during an experiment. Designating a sample by its value of ϕ is merely a convenient way to show that samples with different initial fibre tilt angle display quantitatively different directional pull-off behaviour.

4.2. Initiation of sliding under tensile force

An alternative way to characterize the combined adhesion–friction behaviour of a surface is to measure the critical tangential force necessary to cause separation or sliding under a constant normal tensile force. As described in figure 3, a constant normal tensile force is applied between the sample and the probe sphere while the sample is translated laterally at a constant velocity of 3 μm s^{-1}. As the sample moves, the normal force tends to change; the z-position of the sample is adjusted continuously to maintain a constant normal force until the samples separate. Consider the results shown in figure 8 for the bulk PDMS sample. Figure 8*a* shows the history of the normal force (P) and the tangential force (T) for three values of $P=83.5$, 48.8 and 29.3 mN. Note that the normal pull-off force is 92.2 mN. The dashed lines represent P and show that P was held constant during the experiment, while T, shown by solid lines, increases monotonically until pull-off. As P decreases, the critical tangential force T_c increases gradually, as shown in figure 8*b*. For most of the range of P considered, the relation between T_c and P is almost linear, with significant deviation from linearity only for low values of P, on the left end of the plot. Now consider the results for the vertical fibre sample, shown in figure 9. For values of P close to the pull-off force, the behaviour is similar to the bulk sample, i.e. T_c increases almost linearly with decrease in P, as seen in figure 9*a*,*b* for $P=88.5$, 68.9 and 66.5 mN. However, the response changes radically for a small further drop in P, as shown in figure 9*a* for $P=64.7$ mN, a mere 1.8 mN smaller than the previous value ($P=66.5$ mN). The magnitude of T continues to increase with sliding displacement and with no apparent interfacial slip to a value $T\sim1650$ mN, more than an order of magnitude greater than that for $P=66.5$ mN. During such loading, in the absence of interfacial slip, the fibres get stretched and deformed severely to accommodate the large lateral

displacement. At $T \sim 1650$ mN, further loading was stopped to prevent fibre fracture and sample destruction. It was also observed that, in contrast to the cases of higher P which resulted in pull-off, the area of contact expands with lateral displacement. Thus, at a critical value of P, the sliding response undergoes a sudden transition from a simple pull-off separation to very high sliding resistance with no separation where the fibre strength appears to be the limiting factor, not the interface. The critical value of P at the transition was highly repeatable within ± 2 mN. Also, as expected, the response was symmetric with respect to sliding in either direction. Thus, the film-terminated fibrillar samples show significantly higher sliding resistance compared with bulk samples for tensile normal forces except when they are very close to the pull-off value. Although the detailed mechanics responsible for this behaviour will not be discussed here, it is a consequence of the increased lateral compliance introduced by the fibrillar structure and, more importantly, the increase in the normal compliance of the fibres under the sphere as the lateral displacement is increased. Consider the vertical fibre sample in the current experiment with a given lateral displacement applied to the sphere in contact. The fibres would have deformed from their initial straight configuration to a bent shape, while still satisfying normal slope condition at the top and the bottom. In this deformed geometry, the normal compliance of the bent fibres is higher than that of the initial straight fibres. A further increment in lateral displacement causes the lateral force T to increase, which in turn tends to decrease the area of contact and/or cause relative slip within the area of contact. However, the increment in lateral displacement also causes the fibres to bend more and cause a further increase in their normal compliance. The increase in normal compliance in turn tends to increase the area of contact. The competition between these two effects, mediated by the magnitude of P, determines which sliding behaviour results: pull-off separation or expanding area of contact with no separation. A quantitative description of these ideas will be discussed elsewhere.

Now, consider the results for the 40° sample, shown in figure 10. Sliding the sphere in the direction of fibre tilt and against the tilt is designated as positive and negative, respectively, as indicated in figure 10. The response is observed to be strongly direction dependent. Sliding in the positive direction is similar to that of the vertical fibre samples, showing a sudden shift in T_c at a critical P. Sliding in the negative direction is similar to that of the bulk sample within the range of values of P considered. Thus, the tilted fibre samples display a very interesting 'one-way clutch' like behaviour under tensile normal loads: one direction is highly resistant to sliding compared with the other. Note that, unlike the bulk and vertical fibre samples, T_c is positive for high values of P, even for the negative direction curve (inverted triangles). Positive values of T_c at high normal force P are a consequence of elastic anisotropy of the tilted fibre layer. It is easily understood by considering the extreme right point in figure 10*b*. It corresponds to bringing the sphere into contact with the sample and retracting in the normal direction, without any lateral motion of the sample. Since the fibre layer is elastically anisotropic, normal retraction

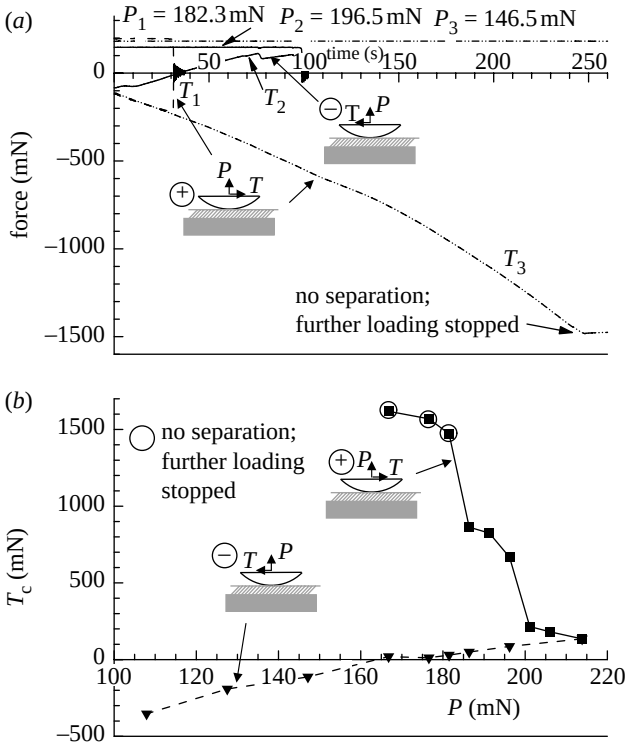

Figure 10. Sliding under tensile force—results for tilted fibre samples ($\phi = 40°$). (*a*) History of normal (P) and tangential (T) forces during sliding. For sliding in positive direction, the behaviour is similar to the vertical fibre samples, i.e. sliding resistance undergoes an almost step change with the normal force P. (*b*) Critical tangential force T_c as a function of normal tensile force P. The response in the negative direction (against the fibre tilt) is similar to that of the bulk PDMS, i.e. T_c increases almost linearly with decrease in P. The estimated measurement error is approximately $\pm 5\%$.

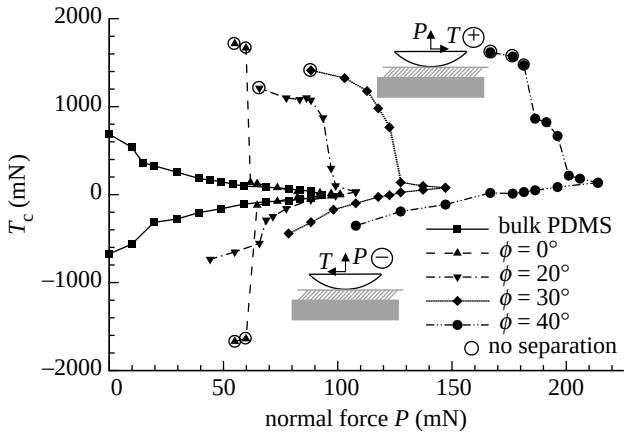

Figure 11. Summary of results for sliding under tensile force experiments, for all cases considered. Data for each case considered have two branches, corresponding to sliding in positive (along the fibre tilt) and negative (against the fibre tilt), respectively. The measurement error for all samples is approximately $\pm 5\%$. The bulk and the vertical fibre sample behaviour is symmetric in positive and negative directions. The behaviour in the two directions is radically different for the tilted fibres, showing very strong anisotropy in sliding resistance.

of the sphere results in both normal and tangential forces. In other words, the extreme right point represents the normal and tangential forces at normal pull-off. Note that, owing to fibre orientation, the tangential force component at pull-off is positive, i.e. acting on the sample to the right. For the negative direction curve, the sphere moves to the left relative to the sample, applying a negative force. Hence, as P is decreased, T_c gradually changes from the initial positive value to negative values. Results for all fibre orientations considered are shown in figure 11, which show that all tilted fibre samples show similar strongly anisotropic response. However, for small values of ϕ, i.e. $\phi = 20°$, even the negative branch shows a sudden increase in T_c for sufficiently low values of P.

5. SUMMARY

This article presents experimental observations of the adhesion and friction responses of surfaces with a film-terminated tilted fibre architecture. The most significant observations of the study are as follows. (i) Detachment force increases significantly with tilt angle; in the case of the 40° sample, it increased by a factor greater than 3 compared with the bulk sample. The results presented here can serve as a starting point to develop a quantitative description of the mechanics of these surfaces and to optimize the geometric parameters for maximum detachment force. (ii) As the angle of tilt increases, the samples display an increasingly sharp minimum at a negative angle, which can serve as the direction of easy detachment. In contrast to the prediction of the analysis of Chen & Gao (2007), no peak in detachment force aligned in the direction of maximum elastic modulus was observed. Some of the possible causes of the deviation could be the dependence of the critical energy release rate on the mode mixity at the contact edge and the finite thickness of the fibrous layer. In addition, the analysis of Chen & Gao (2007) is for a cylinder in contact with an anisotropic half-space, within the framework of small-strain elasticity. Moreover, the axis of anisotropy remains fixed during attachment and detachment. However, the current experiments have a sphere in contact with a discrete fibrous layer of finite thickness, where the fibres can undergo large deflections and rotations during detachment. Such a situation is quite different from that assumed in the analysis. (iii) Under constant tensile normal load, the vertical fibre samples display a fascinating switch from easy pull-off to very strong sliding resistance with a small perturbation in the normal load, almost like a phase transformation. This situation is very different from the response of bulk samples, which shows an almost linear relation between the normal load and the critical tangential force. (iv) The response of the tilted fibre samples under sliding has two branches. In the positive direction along the tilt, they behave similar to the vertical fibre samples, showing the sudden transition from pull-off to no separation. In the negative direction, the response is similar to that of the bulk samples. Thus, the tilted fibre samples display a strong anisotropy in sliding resistance. It is necessary to develop a quantitative description of the above observations to optimize the desired behaviour and develop the considered surface architecture for practical applications.

Funding for this work was provided by a grant from the Mechanics of Multifunctional Materials and Microsystems programme of the Air Force Office of Scientific Research (grant no. FA9550-05-1-0210, programme manager: Dr Les Lee). Also, support from the National Science Foundation (grant no. CMMI-0547032) is gratefully acknowledged.

REFERENCES

Arzt, E., Gorb, S. & Spolenak, R. 2003 From micro to nano contacts in biological attachment devices. *Proc. Natl Acad. Sci. USA* **100**, 10 603–10 606. (doi:10.1073/pnas.1534701100)

Autumn, K., Liang, Y. A., Hsieh, S. T., Zesch, W., Chan, W. P., Kenny, T. W., Fearing, R. & Full, R. J. 2000 Adhesive force of a single gecko foot-hair. *Nature* **405**, 681–685. (doi:10.1038/35015073)

Bhushan, B. & Sayer, R. A. 2007 Surface characterization and friction of a bio-inspired reversible adhesive tape. *Microsyst. Technol.* **13**, 71–78. (doi:10.1007/s00542-006-0256-2)

Bhushan, B., Peressadko, A. G. & Kim, T. W. 2006 Adhesion analysis of two-level hierarchical morphology in natural attachment systems for 'smart adhesion'. *J. Adhes. Sci. Technol.* **20**, 1475–1491. (doi:10.1163/156856106778666408)

Carpick, R. W., Agrait, N., Ogletree, D. F. & Salmeron, M. 1996 Variation of the interfacial shear strength and adhesion of a nanometer-sized contact. *Langmuir* **12**, 3334–3340. (doi:10.1021/la9509007)

Chen, S. & Gao, H. 2007 Bio-inspired mechanics of reversible adhesion: orientation-dependent adhesion strength for non-slipping adhesive contact with transversely isotropic elastic materials. *J. Mech. Phys. Solids* **55**, 1001–1015. (doi:10.1016/j.jmps.2006.10.008)

Crosby, A. J., Hageman, M. & Duncan, A. 2005 Controlling polymer adhesion with "pancakes". *Langmuir* **21**, 11 738–11 743. (doi:10.1021/la051721k)

Gao, H., Ji, B., Jäger, I. L., Arzt, E. & Fratzl, P. 2003 Materials become insensitive to flaws at nanoscale: lessons from nature. *Proc. Natl Acad. Sci. USA* **100**, 5597–5600. (doi:10.1073/pnas.0631609100)

Gao, H., Wang, X., Yao, H., Gorb, S. & Arzt, E. 2005 Mechanics of hierarchical adhesion structures of geckos. *Mech. Mater.* **37**, 275–285. (doi:10.1016/j.mechmat.2004.03.008)

Ge, L., Sethi, S., Ci, L., Ajayan, P. M. & Dhinojwala, A. 2007 Carbon nanotube-based synthetic gecko tapes. *Proc. Natl Acad. Sci. USA* **104**, 10 792–10 795. (doi:10.1073/pnas.0703505104)

Geim, A. K., Dubonos, S. V., Grigorieva, I. V., Novoselov, K. S., Zhukov, A. A. & Shapoval, S. Y. 2003 Microfabricated adhesive mimicking gecko foot-hair. *Nat. Mater.* **2**, 461–463. (doi:10.1038/nmat917)

Glassmaker, N. J., Jagota, A., Hui, C. Y., Noderer, W. L. & Chaudhury, M. K. 2007 Biologically inspired crack trapping for enhanced adhesion. *Proc. Natl Acad. Sci. USA* **104**, 10 786–10 791. (doi:10.1073/pnas.0703762104)

Gorb, S., Varenberg, M., Peressadko, A. & Tuma, J. 2007 Biomimetic mushroom-shaped fibrillar adhesive microstructure. *J. R. Soc. Interface* **4**, 271–275. (doi:10.1098/rsif.2006.0164)

Huber, G., Gorb, S., Spolenak, R. & Arzt, E. 2005 Resolving the nanoscale adhesion of individual gecko spatulae by atomic force microscopy. *Biol. Lett.* **1**, 2–4. (doi:10.1098/rsbl.2004.0254)

Hui, C.-Y., Glassmaker, N. J., Tang, T. & Jagota, A. 2004 Design of biomimetic fibrillar interfaces: 2. Mechanics of enhanced adhesion. *J. R. Soc. Interface* **1**, 35–48. (doi:10.1098/rsif.2004.0005)

Israelachvili, J. 1992 Adhesion, friction and lubrication of molecularly smooth surfaces. In *Fundamentals of friction* (eds I. L. Singer & H. M. Pollock). NATO ASI Series E, pp. 351–385. Dordrecht, The Netherlands: Kluwer Academic Publishers.

Jagota, A. & Bennison, S. J. 2002 Mechanics of adhesion through a fibrillar microstructure. *Integr. Comp. Biol.* **42**, 1140–1145. (doi:10.1093/icb/42.6.1140)

Johnson, K. L. 1997 Adhesion and friction between a smooth elastic spherical asperity and a plane surface. *Proc. R. Soc. A* **453**, 163–179. (doi:10.1098/rspa.1997.0010)

Kim, S. & Sitti, M. 2006 Biologically inspired polymer microfibers with spatulate tips as repeatable fibrillar adhesives. *Appl. Phys. Lett.* **89**, 261 911. (doi:10.1063/1.2424442)

Kim, T. W. & Bhushan, B. 2007 Adhesion analysis of multi-level hierarchical attachment system contacting with a rough surface. *J. Adhes. Sci. Technol.* **21**, 1–20. (doi:10.1163/156856107779976097)

Kim, K. S., McMeeking, R. M. & Johnson, K. L. 1998 Adhesion, slip, cohesive zones and energy fluxes for elastic spheres in contact. *J. Mech. Phys. Solids* **46**, 243–266. (doi:10.1016/S0022-5096(97)00070-7)

Liechti, K. M. & Chai, Y. S. 1992 Asymmetric shielding in interfacial fracture under in-plane shear. *J. Appl. Mech.* **59**, 295–304.

Liu, H. W. & Bhushan, B. 2003 Adhesion and friction studies of microelectromechanical systems/nanoelectromechanical systems materials using a novel microtriboapparatus. *J. Vac. Sci. Technol. A* **21**, 1528–1538. (doi:10.1116/1.1560711)

Northen, M. T. & Turner, K. L. 2005 A batch fabricated biomimetic dry adhesive. *Nanotechnology* **16**, 1159–1166. (doi:10.1088/0957-4484/16/8/030)

Northen, M. T. & Turner, K. L. 2006 Meso-scale adhesion testing of integrated micro- and nano-scale structures. *Sens. Actuators A* **130**, 583–587.

Peressadko, A. & Gorb, S. N. 2004 When less is more: experimental evidence for tenacity enhancement by division of contact area. *J. Adhes.* **80**, 247–261. (doi:10.1080/00218460490430199)

Persson, B. N. J. & Gorb, S. 2003 The effect of surface roughness on the adhesion of elastic plates with application to biological systems. *J. Chem. Phys.* **119**, 11 437–11 444. (doi:10.1063/1.1621854)

Persson, B. N. J., Albohr, O., Tartaglino, U., Volokitin, A. I. & Tosatti, E. 2005 On the nature of surface roughness with application to contact mechanics, sealing, rubber friction and adhesion. *J. Phys. Condens. Matter* **17**, R1–R62. (doi:10.1088/0953-8984/17/1/R01)

Rennie, A. C., Dickrell, P. L. & Sawyer, W. G. 2005 Friction coefficient of soft contact lenses: measurements and modeling. *Tribol. Lett.* **18**, 499–504. (doi:10.1007/s11249-005-3610-0)

Savkoor, A. R. 1987 *Dry adhesive contact of elastomers*. ME dissertation, Delft University of Technology, Delft, The Netherlands.

Sitti, M. & Fearing, R. S. 2003 Synthetic gecko foot-hair micro/nano-structures as dry adhesives. *J. Adhes. Sci. Technol.* **17**, 1055–1073. (doi:10.1163/156856103322113788)

Spolenak, R., Gorb, S. & Arzt, E. 2005*a* Adhesion design maps for bio-inspired attachment systems. *Acta Biomater.* **1**, 5–13. (doi:10.1016/j.actbio.2004.08.004)

Spolenak, R., Gorb, S., Gao, H. & Arzt, E. 2005*b* Effects of contact shape on the scaling of biological attachments. *Proc. R. Soc. A* **461**, 305–319. (doi:10.1098/rspa.2004.1326)

Tang, T., Hui, C.-Y. & Glassmaker, N. J. 2005 Can a fibrillar interface be stronger and tougher than a non-fibrillar one? *J. R. Soc. Interface* **2**, 505–516. (doi:10.1098/rsif.2005.0070)

Tian, Y., Pesika, N., Zeng, H., Rosenberg, K., Zhao, B., McGuiggan, P., Autumn, K. & Israelachvili, J. 2006 Adhesion and friction in gecko toe attachment and detachment. *Proc. Natl Acad. Sci. USA* **103**, 19 320–19 325. (doi:10.1073/pnas.0608841103)

Yao, H. & Gao, H. 2006 Mechanics of robust and releasable adhesion in biology: bottom-up designed hierarchical structures of gecko. *J. Mech. Phys. Solids* **54**, 1120–1146. (doi:10.1016/j.jmps.2006.01.002)

Yurdumakan, B., Raravikar, N. R., Ajayan, P. M. & Dhinojwala, A. 2005 Synthetic gecko foot-hairs from multi-walled carbon nanotubes. A. *Chem. Commun.* **30**, 3799–3801. (doi:10.1039/b506047h)

Zhao, Y., Tong, T., Delzeit, L., Kashani, A., Meyyappan, M. & Majumdar, A. 2006 Interfacial energy and strength of multiwalled-carbon-nanotube-based dry adhesive. *J. Vac. Sci. Technol. B* **24**, 331–335. (doi:10.1116/1.2163891)